Results in Physics 16 (2020) 102839

Contents lists available at ScienceDirect

Results in Physics

journal homepage: www.elsevier.com/locate/rinp

Effect of deep-level defect density of the absorber layer and n/i interface in perovskite solar cells by SCAPS-1D

M.S. Chowdhury[a,b], S.A. Shahahmadi[c], P. Chelvanathan[b], S.K. Tiong[c], N. Amin[c], K. Techato[a,d,g,*], N. Nuthammachot[a], T. Chowdhury[e], M. Suklueng[f]

[a] Sustainable Energy Management, Faculty Environmental Management, Prince of Songkla University, Songkhla, Thailand
[b] Solar Energy Research Institute (SERI), Universiti Kebangsaan Malaysia (UKM), 43600 Bangi, Selangor, Malaysia
[c] Institute of Sustainable Energy (ISE), Universiti Tenaga Nasional (@The National Energy University), Jalan IKRAM-UNITEN, 43000 Kajang, Selangor, Malaysia
[d] Municipal Solid Waste and Hazardous Waste Management, Canter of Excellent on Hazardous Substance Management (H&M), Bangkok, Thailand
[e] Department of #Computer Science and Information Technology, Southern University Bangladesh, Chittagong, Bangladesh
[f] PSU Energy System Research Institute, Prince of Songkla University, Thailand
[g] Environmental Assessment and Technology for Hazardous Waste Management Research Centre, Faculty of Environmental Management, Prince of Songkla University, 90110 Songkhla, Thailand

ARTICLE INFO

Keywords:
Solar cell simulation
Perovskite
Defect density
Interface
SCAPS-1D

ABSTRACT

In this paper, Solar Cell Capacitance Simulator-1D (SCAPS-1D) was used to study the absorber layer defect density and n/i interface of perovskite solar cells versus various cell thickness values. The planar p-i-n structure was defined as PEDOT:PSS/Perovskite/CdS, and its performance was simulated. Power conversion efficiency $> 25\%$ can be achieved at $< 10^{14}$ cm^{-3} defect density and > 400 nm thickness of absorber layer, respectively. The study assumed 0.6 eV Gaussian defect energy level below the perovskite's conduction band with a characteristic energy of 0.1 eV. These conditions resulted in an identical outcome on the n/i interface. These results show constraints on numerical simulation for correlation between defect mechanism and performance.

Introduction

Perovskite solar cell is an emerging area of study in thin-film photovoltaics due to its relatively low-cost and environmentally friendly fabrication. The maximum power conversion efficiency (PCE) of 24.2% is reported recently by Korea Research Institute of Chemical Technology (KRICT) in laboratory [1], which may place perovskite beside the commercialized crystalline silicon (26.7% in laboratory [2]) in future. The perovskite materials employ the 'ABX$_3$' crystal structure, in which the 'A' cation in cubo-octahedral site makes bonding with 'BX$_6$' octahedra. The comparative sizes of the 'A' cation and the 'BX$_6$' octahedra regulate the dimensionality of the perovskite materials. In overall, the small 'A' cation is suitable for photovoltaic applications, which can maintain a three-dimensional structure [3]. Among several combinations of the components, the most common halide perovskite is methylammonium lead iodide (MAPbI3) [4]. Its phase transformation is relatively quick and simple, but its mixed compositions make complicated perovskite solar cells. The stable phase of MAPbI1-xClx is sustainable only if the portion of chlorine replacement is $< 4\%$ due to the large discrepancy in ionic radius between Cl- and I- [5]. These materials are limited by phase isolation under illumination due to halide relocation Hoke's effect, which leads to a high open-circuit voltage (Voc) and consequently causing photo stability [6].

Investigation on perovskite solar cells requires to focus on the improvement of PCE through new deposition techniques to engineer suitable morphological and compositional properties. Unlike well-controlled fabrication in silicon solar cells, perovskite materials are fabricated via one-step or two-step spin-on solution-based method [7]. These methods produce a number of defects during manufacture, which are the fundamental factors that influence productivity and reproducibility. Mid-gap states in a band structure are formed and partake in bearer recombination. The managing trap structure and intensity are significant for achieving reproducible outcomes with high efficiency. The defects are characterized as either of shallow or deep level. Shallow defects, which are inside a couple of thermal energy units of a band edge, do not impede productivity much, as they normally catch only

* Corresponding author at: Faculty of Environmental Management, Prince of Songkla University, PO Box 50, Kho Hong Post Office, Hat Yai District, Songkhla 90112, Thailand.
E-mail address: Kuaanan.t@psu.ac.th (K. Techato).

https://doi.org/10.1016/j.rinp.2019.102839
Received 13 July 2019; Received in revised form 21 November 2019; Accepted 24 November 2019
Available online 27 November 2019

one type of carrier, which is released rather. Deep defects are situated close to the center of the band gap and become increasingly inconvenient, since they catch both types of carriers, thereby permitting enough time for charge transporter recombination [4,8,9]. Yin et al. determined the transition-state energies of all known characteristic point trap in $MAPbI_3$ structures. They discovered that both shallow- and deep-level defects exist within the bandgap [10]. Approximately 10^{10} –10^{11} cm^{-3} are identified as shallow defects with space charge limited current measurements [11], whereas deep level defects are identified with density of 10^{14} –10^{16} cm^{-3} with time-resolved photoluminescence [12], transient photocurrent measurements [13], and deep level transient spectroscopy [14]. Sung Heo et al. [14] fabricated perovskite solar cells using one-pot and cuboid methods. They found that both solar cells have two kinds of deep level defect densities at 0.65 eV (E1) and 0.76 eV (E2) below the conduction band edge regardless of the processing method. The E1 and E2 are known to originate from iodine anti-sites on Pb and MA, respectively [10].

In this study, effect of deep-level defect density on the absorber layer and n/i interface for perovskite solar cells is investigated. The results such as, open-circuit voltage (V_{oc}), short-circuit current (J_{sc}), fill factor (FF), and PCE in p-i-n planar structure were determined by SCAPS-1D simulator.

Simulation methodology

There are different hole transport materials (HTMs) and electron transport materials (ETMs) used in the fabrication of perovskite solar cells. In the case of HTM, triphenylamine [15], Dithieno [3,2-b:2′,3′-d] pyrrole (DTP) derivatives [16], conjugated polymers [17], NiO_x, Spiro-OMeTAD [18], PEDOT:PSS [19] etc. have been applied. Spiro-OMeTAD has been studied by many researchers and received high PCE > 21% [18]. However, its cost and low hole mobility are still the matter of concern [20]. The PEDOT: PSS is generating considerable interest as the charge transport layers, which was used in 2013 for the first time [21]. It has notable characteristics such as high transparency, mechanical stability, excellent flexibility, low-temperature processing, and low conductivity [22]. In 2018, Hytham Elbohy et al. reported the highest PCE of 18% using PEDOT: PSS as the HTM [19]. On the other hand, materials such as TiO_2 [23,24], SnO_2 [25], Zn_2SnO_4 [25], polyethylenimine [26], PCBM [27,28] etc. have been investigated as the ETM. Most studies are focused on TiO_2 and PCBM in perovskite solar cells, which result in a device with low hysteresis and high performance [29,30]. From the fabrication point of view, TiO_2 nanoparticles are annealed at high temperature, while the PCBM is fully compatible with low-temperature solution managing methods. Although differences of opinion still exist, it appears by an agreement that PCBM refers to fullerene-based, which is cost-effective in the industrial scale. Other n-type oxides, such as In_2O_3, and SnO_2 are deposited by sol–gel processes for the planar architecture and do not require the high-temperature calcination step even though the yielded devices suffer from some serious drawbacks. In this study, the common PEDOT:PSS was employed as the HTM for the perovskite layer, whereas the CdS was selected as the ETM [31]. The CdS has higher electron mobility compared to the TiO_2, which results in a lower series resistance in the perovskite solar cells. Its conduction band energy level stays lower than TiO_2 resulted in a higher open-circuit voltage in general [32]. On the other hand, the CdS has a direct band gap of 2.4 eV with an excellent electron transportability. Furthermore, 45 nm thickness experimentally applied on an inverted structure of perovskite solar cell reported by Jia [33]. Table 1 lists the simulation parameters, which were chosen from the literature. It is reported that the PEDOT:PSS thickness is from 30 to 130 nm, whereas its band gap at 2.2 eV is optimum. In overall, we can say that optoelectrical properties of layers are highly dependent on the layer thickness, deposition methods, and measurement techniques. Defining accurate material properties based on the variation of thickness is very difficult and subjective [34,35]. For example, various different values for dielectric permeability is reported in the literature, which can be correlated to potential instability of a crystalline lattice in complex perovskites [36]. Moreover, defects change the optoelectrical properties of a material system and the experimental study about a correlation between defects and optoelectrical properties has lots of challenges apart from the need of exceedingly sophisticated equipment, which is not accessible in many groups. This issue causes undeveloped modeling and, in consequence, defects are disregarded in majority of reported simulations. Although many scientists accept variations in optoelectrical properties while defects are constant with certain values [37]. However, understanding about individual defects' mechanism in simulation software with a constant optoelectrical properties has not been revealed yet. Therefore, influence of the defect density in both absorber and n/i interface layer of perovskite solar cells in various perovskite thickness is investigate with an assumption of constant optoelectrical properties. SCAPS-1D (version 3.3.01) was used to simulate the perovskite planar structure Au/PEDOT:PSS/Perovskite/CdS/TCO/Glass in this study as shown in Fig. 1. SCAPS-1D is a one dimensional solar cell simulation programme specifically developed for thin film solar cell operation and later extended for crystalline solar cells (Si and GaAs family) and amorphous cells (a-Si and micromorphous Si) [38]. Recently, Minemoto et. al successfully demonstrated the ability of SCAPS-1D to numerically simulate the performance perovskite solar cells [39]. Among the salient features of SCAPS-1D, which render it appropriate for this study is its ability to simulate cell structure with various complex defect configurations such as bulk or interface, charge type (no charge, monovalent, divalent or amphoteric), energetic distribution (single level, uniform, Gauss, tail, or combinations) [40,41].

Results and discussion

The band diagram of the p-i-n perovskite solar cell in equilibrium condition is shown in Fig. 1. The defect energy level at 0.6 eV is present below the conduction band (E_c) of the absorber layer. Fig. 2 shows contour graphs of perovskite solar cell performance parameters dependency on of absorber defect density and thickness variables. The effect of deep-defect density from 10^{11} to 10^{17} cm^{-3} and thickness from 300 to 1000 nm are analysed to assess the device performance. As shown, the Voc varied from 0.86 to 1.21 V, and device performance strongly depends on the defect density mostly. The highest 1.21 V, V_{oc} is achieved at thickness < 400 nm and defect density < 10^{13} cm^{-3}. Upon the increase of defect density > 10^{14} and thickness > 500 nm, the V_{oc} decreases rapidly in the vicinity of 1.15 and then reduces gradually to 0.86 V. In contrast, the J_{sc} shows the highest value > 27 mA/cm^2 at thickness and defect density of > 800 nm and < 10^{15} cm^{-3}, respectively. The decrease in thickness from 500 to 300 nm causes an abrupt drop in the J_{sc} from 25 to 22 mA/cm^2, while similar tendency can be observed at defect > 10^{15} cm^{-3}. The FF is a function of V_{oc} and the recombination processes in the depletion region [50]. Therefore, a similar trend can be found compared to the Voc. The FF > 80% is shown at defect density < 10^{14} cm^{-3}, which is not influenced by the thickness. Conclusively, PCE = V_{oc} × J_{sc} × FF equation suggests that the efficiency is a merger of the three output parameters. The highest PCE of > 25% is observed at thickness > 400 nm and defect density < 10^{14} cm^{-3}. The thickness < 400 nm drops the PCE from 25 to 20%, while defect density > 10^{14} cm^{-3} causes significant reduction in performance all the way down to below 10%.

Fig. 3 shows the impact of interfacial defect density of CdS/Perovskite layer on the device performance. The defect energy level at 0.6 eV is present below the E_c of the CdS layer. Interestingly, the overall trend is very similar to the previous results. However, the device become very prone to the defect density compared to the previous results. Generally, the previous threshold of 10^{14} cm^{-3} for defect density is reduced to 10^{11} cm^{-3}. The highest 1.20 V is obtained in very small region with absorber thickness < 500 nm and CdS/perovskite interface defect density of < 10^{11} cm^{-3}. The V_{oc} reduces outside of

Table 1
List of simulation parameter for perovskite planar structure.

Parameter	PEDOT: PSS	Interface	CH3NH3PbI$_{3-x}$ Cl$_x$	CdS
Thickness (nm)	33		300–1000	45
Bandgap (eV), Eg	2.2 [42]		1.50 [37]	2.4 [43]
Electron Affinity (eV), λ	2.9 [42]		3.9 [44]	4.50 [45]
Dielectric Permittivity (relative), ε_r	3 [46]		10 [47]	10 [45]
Effective Conduction Band Density (cm^{-3}), N_c	2.2×10^{15} [46]		2.75×10^{18} [47]	2.2×10^{18} [45]
Effective Valence Band Density (cm^{-3}), N_v	1.8×10^{18} [46]		3.9×10^{18} [47]	1.9×10^{19} [45]
Electron Mobility (cm^2 /V. S), μn	10 [46]		10 [48]	350 [44]
Hole Mobility (cm^2/V. S), μp	10 [46]		10 [48]	25 [49]
Acceptor Concentration NA (cm^{-3})	3.17×10^{14} [46]		1.0×10^{9} [6]	0
Donor Concentration ND (cm^{-3})	0		1.0×10^{9} [6]	1×10^{18} [44]
Radiative recombination coefficient (cm^3/s)	2.3×10^{-9}	3.0×10^{-11}	3.0×10^{-11}	2.3×10^{-9}
Capture Cross Section for Electrons and Holes (cm^2)		10^{-19}	10^{-15}	
Gaussian Defect Energy Level below perovskite's conduction band (eV)		0.6	0.6	
Characteristics Energy (eV)		0.1	0.1	
Defect density (cm^{-3})	1×10^{14}	$10^{10} - 10^{16}$	$10^{11} - 10^{17}$	1×10^{14}

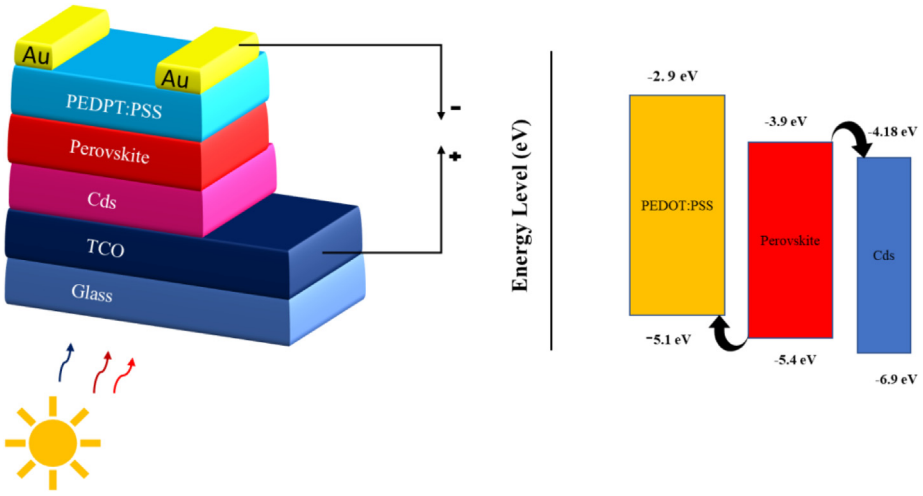

Fig. 1. Schematic diagram of perovskite solar cell and its energy band level.

aforesaid region and its lowest value 0.95 V, calculated at $> 10^{15}$ cm^{-3}. The J_{sc} seems that it is almost independent of defect density and its value increases from 22 to 27 mA/cm^2 while absorber thickness increases from 300 to 1000 nm. Absorber layer thickness has no effect on the FF, and defect density $> 10^{13}$ cm^{-3} can cause rapid decrement on FF around 50%. Finally, the maximum PCE of 28% is observed at thickness and defect density of $>$ 700 nm and $< 10^{11}$ cm^{-3}, respectively. From the experimental view, high series resistance linked to the CdS/absorber interface is regarded as the major consequence of low efficiency of CdS film-based perovskite solar cell [51]. This is attributed to the diffusion of metal cations into the halide perovskite during fabrication step. Structural defects of two unique materials prompts major interfacial deformities, which cause charge recombination in the device.

Herein, we provide an explanation from theoretical point of view, the carrier lifetime (τ) is denoted as the time duration in which a charge carrier is free to move, thus it can contribute to the electric conduction. In a uniform excitation, G electron-hole pairs in the perovskite are generated. Therefore, the generated electron and hole densities in the Ec and Ev are shown in Eqs. (1) and (2) [52], respectively.

$$\Delta n = G\tau_n \tag{1}$$

$$\Delta p = G\tau_p \tag{2}$$

If these carriers are trapped in perovskite, and then thermally re-excited, the time spent in the traps is not included in τ_n and τ_p. In the steady state, the rate of generation in perovskite is equal to the rate of trapping as equation (3) and (4) show [52].

$$\tau_n = \frac{1}{\sigma_p . \nu_{th} . (N_t - n_r)} \tag{3}$$

$$\tau_p = \frac{1}{\sigma_p . \nu_{th} . n_r} \tag{4}$$

where, N_t, n_r, σ_n, and ν_{th} are the total (occupied and unoccupied), the occupied defects, hole capture cross section, thermal velocity. Based on Eqs. (3) and (4), the increase in defect density reduces the carrier lifetime and consequently, results in a shorter carrier diffusion length (L) [53]. The quality of perovskite defines the L, and if the value of L is more than the perovskite thickness, then the device performance would be superior. The relation between L and recombination current (J_o) and V_{oc} is as follows;

$$J_o \approx q\frac{Dn_i^2}{LN} \tag{5}$$

$$V_{oc} = \frac{KT}{q}\ln\left(\frac{J_{sc}}{J_o} + 1\right) \tag{6}$$

From Eq. (5) and (6), we can conclude that the decrease in defect density can decrease the recombination current, and causes an enhancement in the V_{oc}, which is in agreement with our obtained results. On the other hand, the Jsc and the internal quantum efficiency (IQE) are called directly proportional to each other. If we assume a shallow junction solar cells with long minority carrier lifetimes in the perovskite, the IQE can rely on minority carrier diffusion lengths as shown in Eq. (7) [54].

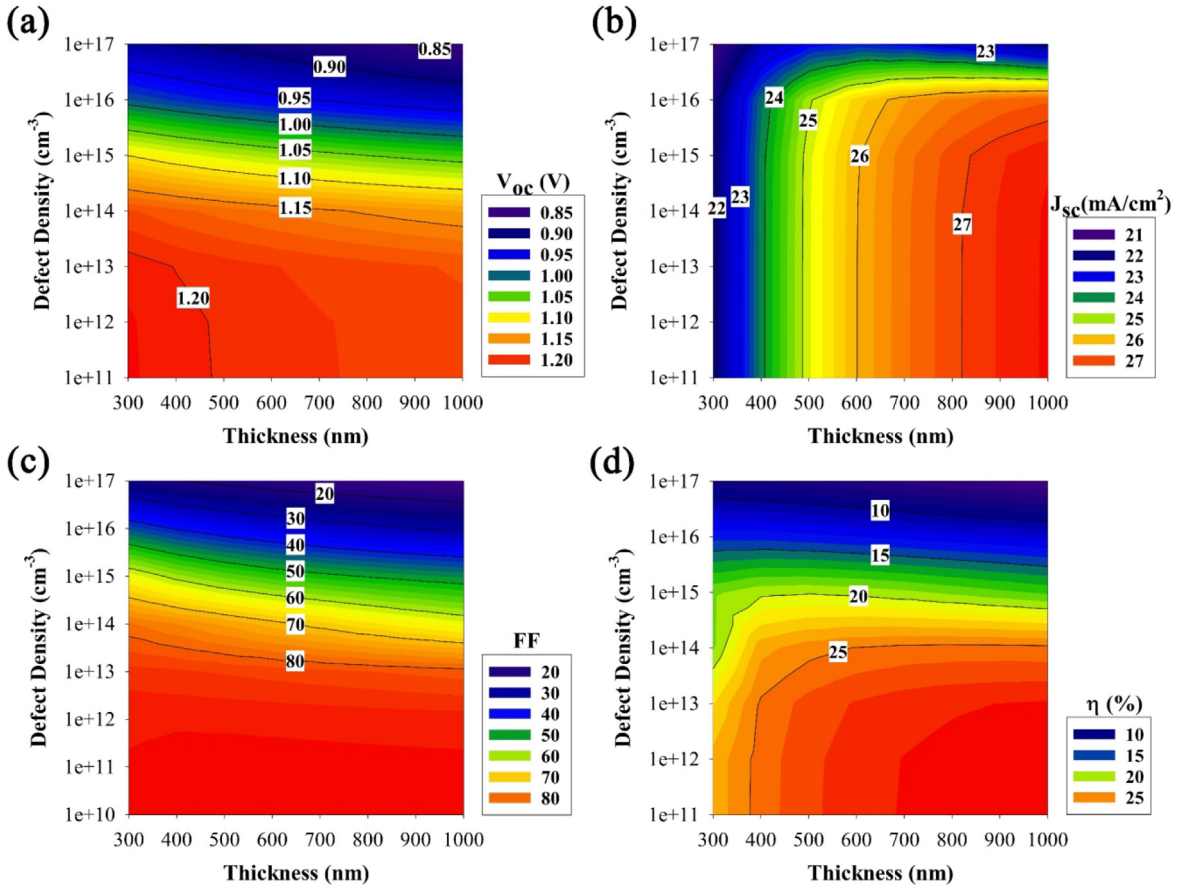

Fig. 2. Contour graphs of perovskite solar cell performance parameters dependency on of absorber defect density and thickness.

$$IQE = 1 - \alpha t - \frac{B}{\alpha L^2} \tag{7}$$

where α, t, and B are denoted as the spectral absorption coefficient, the distance into the perovskite material and perovskite thickness. The Eq. (7) shows the defect density has adverse effect on Jsc. Baena et al. examined carrier density and open-circuit voltage controlled by the bulk charge density and they found that the high-efficiency perovskite solar cell behaves very closely to a bulk recombination ideal photovoltaic model [7]. The Shockley-Read-Hall (SRH) recombination may clarify the conceivable recombination components to decide the impact of defect density on the perovskite solar cell, which is shown as follows;

$$\Re^{SRH} = \frac{\vartheta \sigma_n \sigma_p N_T [np - n_i^2]}{\sigma_p [p + p_1] + \sigma_n [n + n_1]} \tag{8}$$

where ϑ is electron thermal velocity, N_T number of defects per volume, n_i intrinsic number density, n & p are the concentrations of electron and hole at equilibrium and n_1 and p_1 are the concentrations of electrons and holes in trap defect and valence band, respectively. Therefore, it is clear that the defect density has the detrimental effect on perovskite solar cells, and we found that the increase of absorber layer thickness can be a remedy to this issue.

Conclusion

This study optimised perovskite solar cell with a p-i-n configuration using SCAPS simulator. TCO/CdS/Perovskite/PEDOT:PSS structure was the primary modelled solar cell. Candidate materials of 300–1000 nm absorber layer thickness and 10^{11}–10^{17} cm^{-3} absorber layer defect density at the energy level of 0.6 eV. Based on the simulation result, the PCE > 25% was obtained with V_{oc} of 1.2 V, FF 85%, and J_{sc} > 27 mA/cm^2. Increase in absorber layer thickness caused the perovskite solar cell efficiency to rapidly increase. Suitable absorber thickness > 400 nm and defect density of < 10^{14} cm^{-3} were found to be optimal. In the second part, we obtained the CdS/absorber layer thickness. We changed the absorber layer thickness (300–1000 nm) and tuned the defect density (10^{10}–10^{16} cm^{-3}) but maintained the same energy level (0.6 eV). A similar trend was observed although the device performance was more prone to the defect density. We found that the defect density has the detrimental effect on perovskite solar cells, and increasing the thickness of absorber layer up to the certain point can overcome this issue. Our work could provide important guidance for device design and optimisation for perovskite solar cells.

Declaration of Competing Interest

The authors declare that they have no known competing financial interests or personal relationships that could have appeared to influence the work reported in this paper

Acknowledgement

The authors would like to acknowledge the contribution of Thailand's Education Hub for Southern Region of ASEAN Countries Project (THE-AC) code THE-AC 062/2017, and appreciate the support of the Solar Energy Research Institute of Universiti Kebangsaan Malaysia. Due appreciation is also credited to the Institute of Sustainable Energy (ISE) of the Universiti Tenaga Nasional (@The National Energy University) for their cordial support through the research grant number FRGS/1/2018/STG07/UNITEN/01/2. The authors are also thankful to Municipal Solid Waste and Hazardous Waste Management Program for there support.

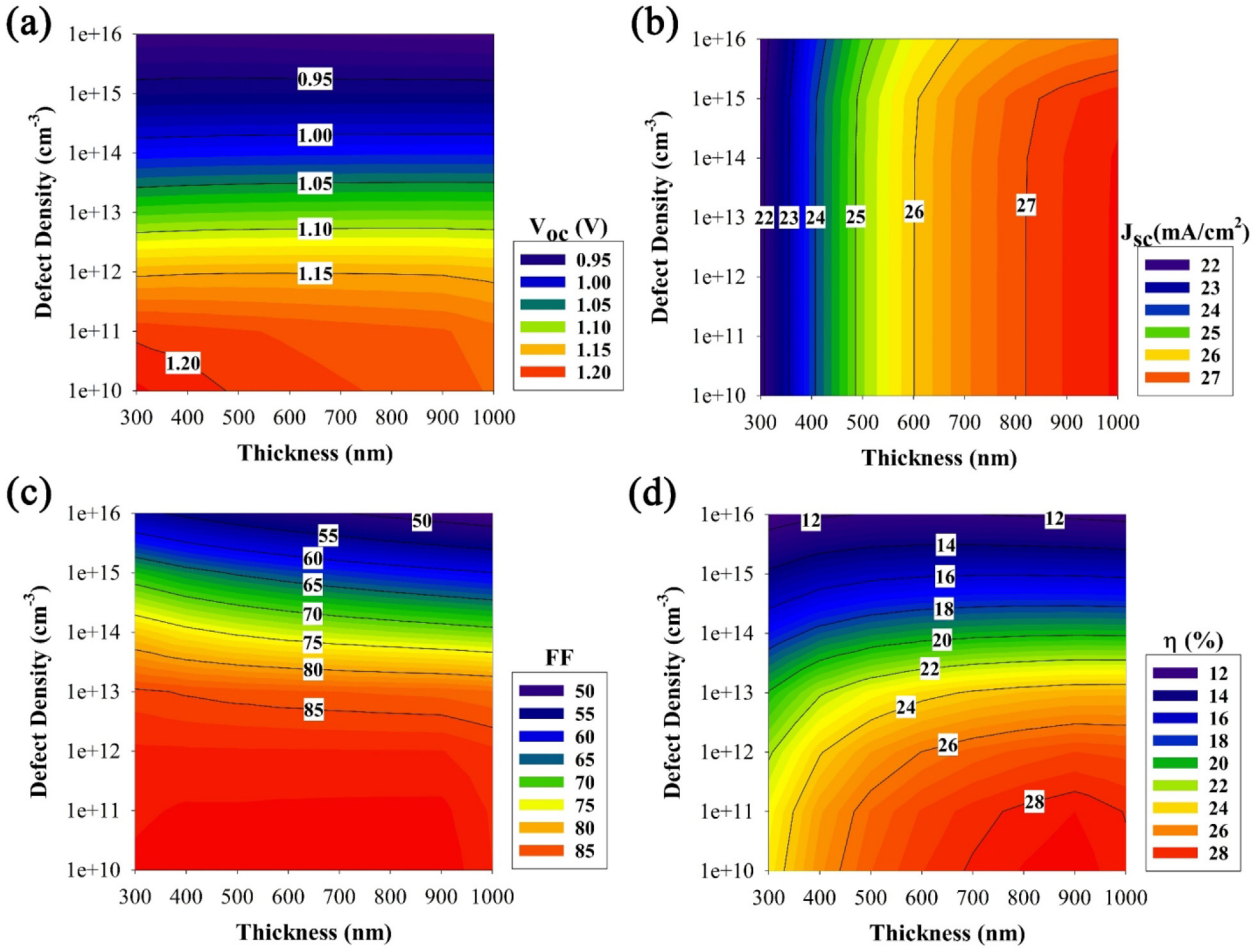

Fig. 3. Contour graphs of perovskite solar cell performance parameters dependency on of defect density of CdS/perovskite interface and perovskite's thickness.

Appendix A. Supplementary data

Supplementary data to this article can be found online at https://doi.org/10.1016/j.rinp.2019.102839.

References

[1] Jung EH, Jeon NJ, Park EY, Moon CS, Shin TJ, Yang T-Y, et al. Efficient, stable and scalable perovskite solar cells using poly(3-hexylthiophene). Nature 2019;567(7749):511–5.

[2] Yoshikawa K, Kawasaki H, Yoshida W, Irie T, Konishi K, Nakano K, et al. Silicon heterojunction solar cell with interdigitated back contacts for a photoconversion efficiency over 26%. Nat Energy 2017;2(5):17032.

[3] Stoumpos CC, Malliakas CD, Kanatzidis MG. Semiconducting Tin and Lead Iodide Perovskites with Organic Cations: Phase Transitions, High Mobilities, and Near-Infrared Photoluminescent Properties. Inorg Chem 2013;52(15):9019–38.

[4] Kearney K, Seo G, Matsushima T, Adachi C, Ertekin E, Rockett A. Computational Analysis of the Interplay between Deep Level Traps and Perovskite Solar Cell Efficiency. J Am Chem Soc 2018;140(46):15655–60.

[5] Wu Y, Islam A, Yang X, Qin C, Liu J, Zhang K, et al. Retarding the crystallization of PbI2 for highly reproducible planar-structured perovskite solar cells via sequential deposition. Energy Environ Sci 2014;7(9):2934–8.

[6] Jamal MS, Shahahmadi SA, Chelvanathan P, Alharbi HF, Karim MR, Ahmad Dar M, et al. Effects of growth temperature on the photovoltaic properties of RF sputtered undoped NiO thin films. Results Phys 2019;14:102360.

[7] Correa-Baena J-P, Turren-Cruz S-H, Tress W, Hagfeldt A, Aranda C, Shooshtari L, et al. Changes from Bulk to Surface Recombination Mechanisms between Pristine and Cycled Perovskite Solar Cells. ACS Energy Lett 2017;2(3):681–8.

[8] Joshi P, Zhang L, Kottokkaran R, Abbas H, Hossain I, Nehra S, et al., editors. Physics of instability of perovskite solar cells. 2016 IEEE 43rd Photovoltaic Specialists Conference (PVSC); 2016 5-10 June 2016.

[9] Joshi PH, Zhang L, Hossain IM, Abbas HA, Kottokkaran R, Nehra SP, et al. The physics of photon induced degradation of perovskite solar cells. AIP Adv 2016;6(11):115114.

[10] Yin W-J, Shi T, Yan Y. Unique Properties of Halide Perovskites as Possible Origins of the Superior Solar Cell Performance. Adv Mater 2014;26(27):4653–8.

[11] Adinolfi V, Yuan M, Comin R, Thibau ES, Shi D, Saidaminov MI, et al. The In-Gap Electronic State Spectrum of Methylammonium Lead Iodide Single-Crystal Perovskites. Adv Mater 2016;28(17):3406–10.

[12] de Quilettes DW, Vorpahl SM, Stranks SD, Nagaoka H, Eperon GE, Ziffer ME, et al. Impact of microstructure on local carrier lifetime in perovskite solar cells. Science 2015;348(6235):683–6.

[13] Leijtens T, Eperon GE, Barker AJ, Grancini G, Zhang W, Ball JM, et al. Carrier trapping and recombination: the role of defect physics in enhancing the open circuit voltage of metal halide perovskite solar cells. Energy Environ Sci 2016;9(11):3472–81.

[14] Heo S, Seo G, Lee Y, Lee D, Seol M, Lee J, et al. Deep level trapped defect analysis in CH3NH3PbI3 perovskite solar cells by deep level transient spectroscopy. Energy Environ Sci 2017;10(5):1128–33.

[15] Zhou P, Fang Z, Zhou W, Qiao Q, Wang M, Chen T, et al. Nonconjugated Polymer Poly(vinylpyrrolidone) as an Efficient Interlayer Promoting Electron Transport for Perovskite Solar Cells. ACS Appl Mater Interfaces 2017;9(38):32957–64.

[16] Mabrouk S, Zhang M, Wang Z, Liang M, Bahrami B, Wu Y, et al. Dithieno[3,2-b:2′,3′-d]pyrrole-based hole transport materials for perovskite solar cells with efficiencies over 18%. J Mater Chem A 2018;6(17):7950–8.

[17] Dubey A, Adhikari N, Venkatesan S, Gu S, Khatiwada D, Wang Q, et al. Solution processed pristine PDPP3T polymer as hole transport layer for efficient perovskite solar cells with slower degradation. Sol Energy Mater Sol Cells 2016;145:193–9.

[18] Wu Y, Wang Z, Liang M, Cheng H, Li M, Liu L, et al. Influence of Nonfused Cores on the Photovoltaic Performance of Linear Triphenylamine-Based Hole-Transporting Materials for Perovskite Solar Cells. ACS Appl Mater Interfaces 2018;10(21):17883–95.

[19] Elbohy H, Bahrami B, Mabrouk S, Reza KM, Gurung A, Pathak R, et al. Tuning Hole Transport Layer Using Urea for High-Performance Perovskite Solar Cells. Advanced Functional Materials.0(0):1806740.

[20] Sherkar TS, Momblona C, Gil-Escrig L, Ávila J, Sessolo M, Bolink HJ, et al. Recombination in Perovskite Solar Cells: Significance of Grain Boundaries, Interface Traps, and Defect Ions. ACS Energy Lett 2017;2(5):1214–22.

[21] Reza KM, Mabrouk S, Qiao Q. A Review on Tailoring PEDOT:PSS Layer for Improved Performance of Perovskite Solar Cells. Proceedings of the Nature Research Society. 2018;2:02004.

[22] Zhou L, Yu M, Chen X, Nie S, Lai W-Y, Su W, et al. Ito-Free Flexible Electronics: Screen-Printed Poly(3,4-Ethylenedioxythiophene): Poly(Styrenesulfonate) Grids as

ITO-Free Anodes for Flexible Organic Light-Emitting Diodes (Adv. Funct. Mater. 11/2018). Adv Funct Mater 2018;28(11)::1870072.
[23] Mabrouk S, Bahrami B, Gurung A, Reza KM, Adhikari N, Dubey A, et al. Higher efficiency perovskite solar cells using additives of LiI, LiTFSI and BMImI in the PbI2 precursor. Sustainable Energy Fuels 2017;1(10):2162–71.
[24] Mabrouk S, Dubey A, Zhang W, Adhikari N, Bahrami B, Hasan MN, et al. Increased Efficiency for Perovskite Photovoltaics via Doping the PbI2 Layer. The Journal of Physical Chemistry C. 2016;120(43):24577–82.
[25] Wu Q, Zhou W, Liu Q, Zhou P, Chen T, Lu Y, et al. Solution-Processable Ionic Liquid as an Independent or Modifying Electron Transport Layer for High-Efficiency Perovskite Solar Cells. ACS Appl Mater Interfaces 2016;8(50):34464–73.
[26] Song S, Moon BJ, Hörantner MT, Lim J, Kang G, Park M, et al. Interfacial electron accumulation for efficient homo-junction perovskite solar cells. Nano Energy 2016;28:269–76.
[27] Yuan Y, Chae J, Shao Y, Wang Q, Xiao Z, Centrone A, et al. Photovoltaic Switching Mechanism in Lateral Structure Hybrid Perovskite Solar Cells. Adv Energy Mater 2015;5(15):1500615.
[28] McMeekin DP, Sadoughi G, Rehman W, Eperon GE, Saliba M, Hörantner MT, et al. A mixed-cation lead mixed-halide perovskite absorber for tandem solar cells. Science 2016;351(6269):151–5.
[29] Wu F, Bahrami B, Chen K, Mabrouk S, Pathak R, Tong Y, et al. Bias-Dependent Normal and Inverted J-V Hysteresis in Perovskite Solar Cells. ACS Appl Mater Interfaces 2018;10(30):25604–13.
[30] Wu F, Pathak R, Chen K, Wang G, Bahrami B, Zhang W-H, et al. Inverted Current-Voltage Hysteresis in Perovskite Solar Cells. ACS Energy Lett 2018;3(10):2457–60.
[31] Dunlap-Shohl WA, Younts R, Gautam B, Gundogdu K, Mitzi DB. Effects of Cd Diffusion and Doping in High-Performance Perovskite Solar Cells Using CdS as Electron Transport Layer. The Journal of Physical Chemistry C. 2016;120(30):16437–45.
[32] Peng H, Sun W, Li Y, Yan W, Yu P, Zhou H, et al. High-performance cadmium sulphide-based planar perovskite solar cell and the cadmium sulphide/perovskite interfaces. J Photonics Energy 2016;6(2):1–13.
[33] Jia J, Wu J, Dong J, Fan L, Huang M, Lin J, et al. Cadmium sulfide as an efficient electron transport material for inverted planar perovskite solar cells. Chem Commun 2018;54(25):3170–3.
[34] Ferdaous MT, Shahahmadi SA, Chelvanathan P, Akhtaruzzaman M, Alharbi FH, Sopian K, et al. Elucidating the role of interfacial MoS2 layer in Cu2ZnSnS4 thin film solar cells by numerical analysis. Sol Energy 2019;178:162–72.
[35] Shahahmadi S, Yeganeh B, Huda N, Asim N, Hafidz M, Alam M, et al. Properties of a-SiGe thin films on glass by co-sputtering for photovoltaic absorber application. J Nanosci Nanotechnol 2015;15(11):9275–80.
[36] Gvasaliya SN, Lushnikov SG, Sashin IL, Shaplygina TA. Density of vibration states and ferroelectric properties of complex perovskites. J Appl Phys 2003;94(2):1130–3.
[37] Jamal MS, Shahahmadi SA, Abdul Wadi MA, Chelvanathan P, Asim N, Misran H, et al. Effect of defect density and energy level mismatch on the performance of perovskite solar cells by numerical simulation. Optik. 2019;182:1204–10.
[38] Burgelman M, Nollet P, Degrave S. Modelling polycrystalline semiconductor solar cells. Thin Solid Films 2000;361:527–32.
[39] Minemoto T, Murata M. Device modeling of perovskite solar cells based on structural similarity with thin film inorganic semiconductor solar cells. J Appl Phys 2014;116(5):054505.
[40] Burgelman M, Decock K, Khelifi S, Abass A. Advanced electrical simulation of thin film solar cells. Thin Solid Films 2013;535:296–301.
[41] Decock K, Zabierowski P, Burgelman M. Modeling metastabilities in chalcopyrite-based thin film solar cells. J Appl Phys 2012;111(4):043703.
[42] Singh R, Singh PK, Bhattacharya B, Rhee H-W. Review of current progress in inorganic hole-transport materials for perovskite solar cells. Appl Mater Today 2019;14:175–200.
[43] Sobayel K, Akhtaruzzaman M, Rahman KS, Ferdaous MT, Al-Mutairi ZA, Alharbi HF, et al. A comprehensive defect study of tungsten disulfide (WS2) as electron transport layer in perovskite solar cells by numerical simulation. Results Phys 2019;12:1097–103.
[44] Kim J, Hou B, Park C, Bahn CB, Hoffman J, Black J, et al. Effect of defects on reaction of NiO surface with Pb-contained solution. Sci Rep 2017;7:44805.
[45] Giorgi G, Fujisawa J-I, Segawa H, Yamashita K. Small Photocarrier Effective Masses Featuring Ambipolar Transport in Methylammonium Lead Iodide Perovskite: A Density Functional Analysis. J Phys Chem Lett 2013;4(24):4213–6.
[46] Konstantakou M, Stergiopoulos T. A critical review on tin halide perovskite solar cells. J Mater Chem A 2017;5(23):11518–49.
[47] Teyou Ngoupo A, Ouédraogo S, Ndjaka JM. Numerical analysis of interface properties effects in CdTe/CdS: O thin film solar cell by SCAPS-1D. Indian J Phys 2019;93(7):869–81.
[48] Azri F, Meftah A, Sengouga N, Meftah A. Electron and hole transport layers optimization by numerical simulation of a perovskite solar cell. Sol Energy 2019;181:372–8.
[49] Homes CC, Vogt T, Shapiro SM, Wakimoto S, Ramirez AP. Optical Response of High-Dielectric-Constant Perovskite-Related Oxide. Science 2001;293(5530):673–6.
[50] Hossain ES, Chelvanathan P, Shahahmadi SA, Sopian K, Bais B, Amin N. Performance assessment of Cu2SnS3 (CTS) based thin film solar cells by AMPS-1D. Curr Appl Phys 2018;18(1):79–89.
[51] Gu Z, Chen F, Zhang X, Liu Y, Fan C, Wu G, et al. Novel planar heterostructure perovskite solar cells with CdS nanorods array as electron transport layer. Sol Energy Mater Sol Cells 2015;140:396–404.
[52] Kao KC. 7 - Electrical Conduction and Photoconduction. In: Kao KC, editor. Dielectric Phenomena in Solids. San Diego: Academic Press; 2004. p. 381–514.
[53] Sridharan A, Noel NK, Hwang H, Hafezian S, Rand BP, Kéna-Cohen S. Time-resolved imaging of non-diffusive carrier transport in long-lifetime halide perovskite thin films. arXiv preprint arXiv:190511242. 2019.
[54] Geist J. Quantum efficiency of the p-n junction in silicon as an absolute radiometric standard. Appl Opt 1979;18(6):760–2.